ELECTRONIC SUPPLEMENTARY INFORMATION FOR

Luminescent Macroporous Aerogels of Two-Dimensional Nanocrystals of Metal Halide Perovskites with Adjustable Semiconducting Bandgaps

Penghao Guo, [a] Xuelian Jiang [a] and Pei-Xi Wang *[a]

[a] i-Lab, Suzhou Institute of Nano-Tech and Nano-Bionics of the Chinese Academy of Sciences, 398 Ruoshui Road, Suzhou, Jiangsu 215123, P. R. China

*Correspondence: pxwang2020@sinano.ac.cn

EXPERIMENTAL METHODS

Materials

Lead(II) oxide (99.0 %, Sigma-Aldrich), 2-phenylethylamine (99.0 %, Sigma-Aldrich), hydrobromic acid (48 wt.% in H_2O, Sigma-Aldrich), hydroiodic acid (57 wt.% in H_2O, 99.95%, Sigma-Aldrich), manganese(II) bromide (anhydrous, 99%, Thermo Scientific Chemicals), N,N-dimethylformamide (anhydrous, 99.8%, Sigma-Aldrich), cis-1-amino-9-octadecene (oleylamine; 98 %, Aldrich), cis-9-octadecenoic acid (oleic acid; 99 %, Sigma-Aldrich), chlorobenzene (anhydrous, 99.8 %, Sigma-Aldrich), and cyclohexane (anhydrous, 99.5 %, Sigma-Aldrich) were used as received.

Characterizations

Atomic force microscopy was conducted on a Bruker Dimension Icon Atomic Force Microscope with ScanAsyst. Field emission scanning electron spectroscopy were performed on a Hitachi Regulus 8230 Ultra-high Resolution Scanning Electron Microscope. Powder X-ray diffraction patterns were collected on a Bruker D8 ADVANCE Diffractometer using copper K-alpha radiation (with a wavelength of 0.15406 nm). Photoluminescence excitation and emission spectroscopy were performed on a Hitachi F-4600 Fluorescence Spectrophotometer.

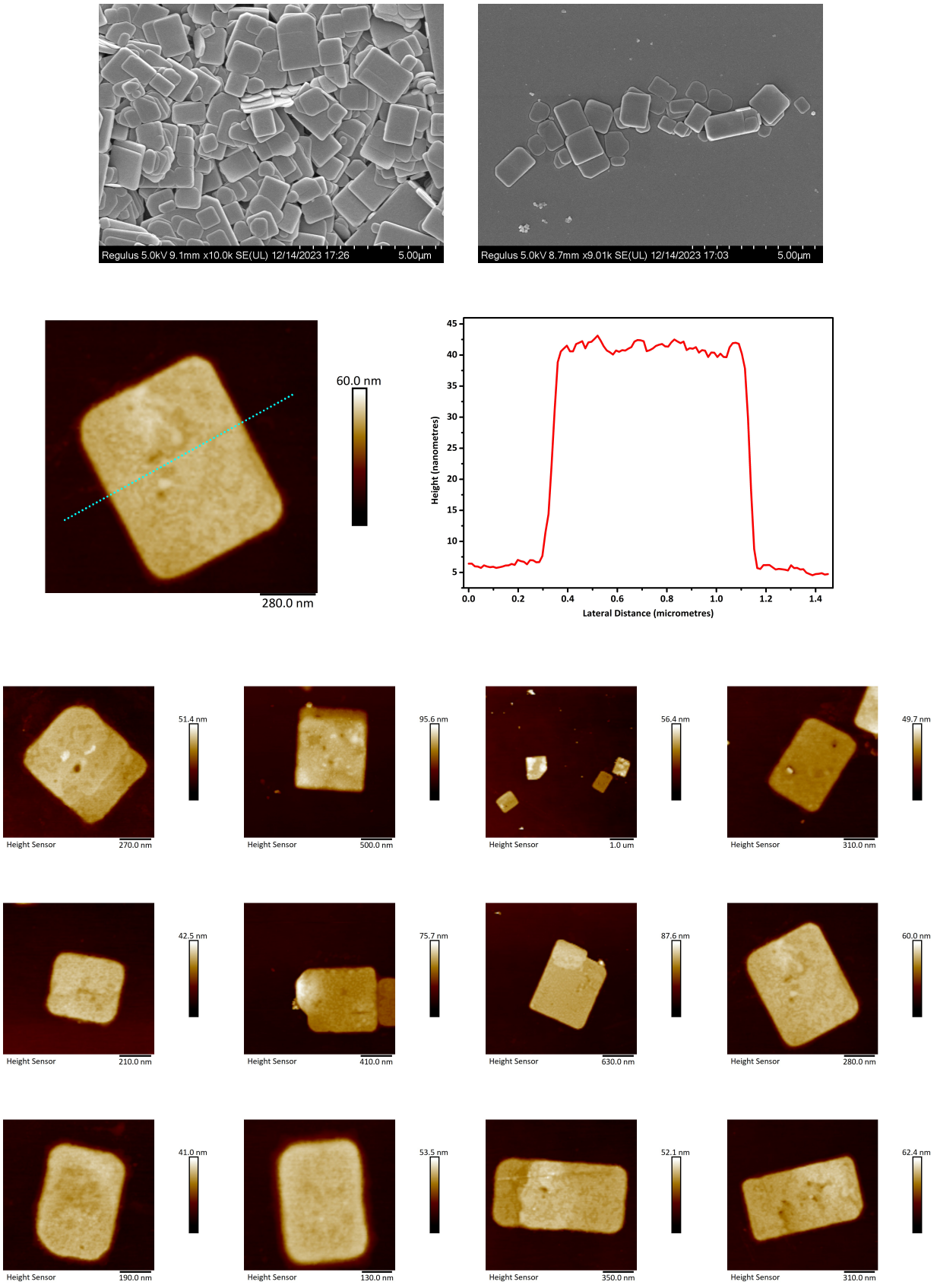

Figure S1. Additional scanning electron microscopy and atomic force microscopy images (with original resolutions of 1320 x 1080 pixels) showing lateral dimensions and thicknesses of $(C_6H_5\text{-}CH_2\text{-}CH_2\text{-}NH_3)_2PbBr_4$ nanoplatelets.

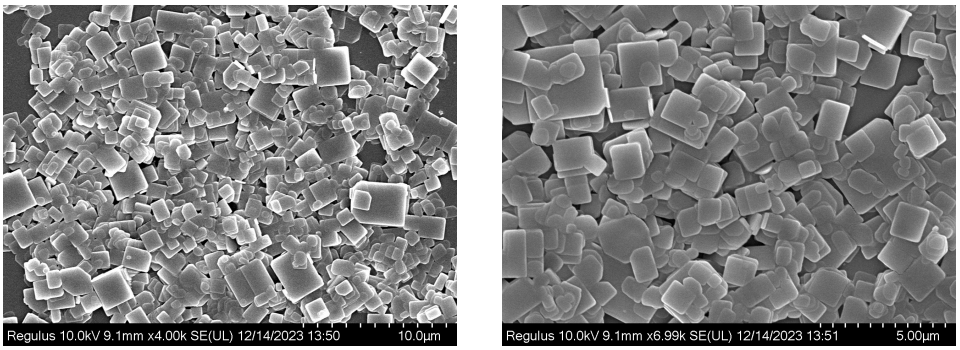

Figure S2. Scanning electron microscopy images showing $(C_6H_5\text{-}CH_2\text{-}CH_2\text{-}NH_3)_2Pb_{0.977}Mn_{0.023}Br_4$ nanoplatelets.

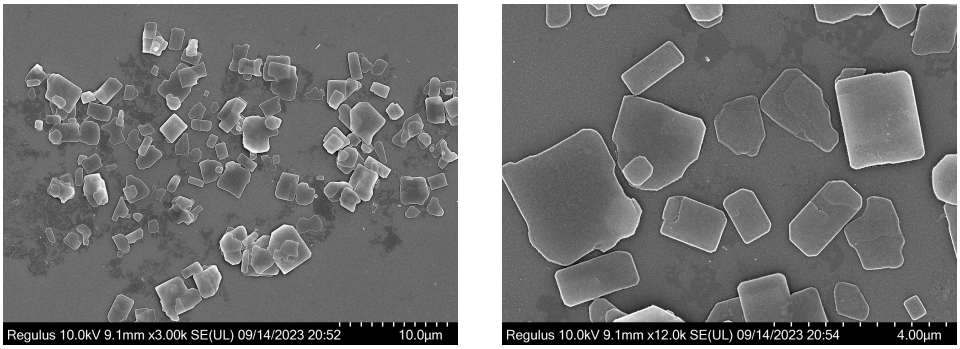

Figure S3. Scanning electron microscopy images showing the geometry of $(C_6H_5\text{-}CH_2\text{-}CH_2\text{-}NH_3)_2PbBr_3I_1$ nanoplatelets.

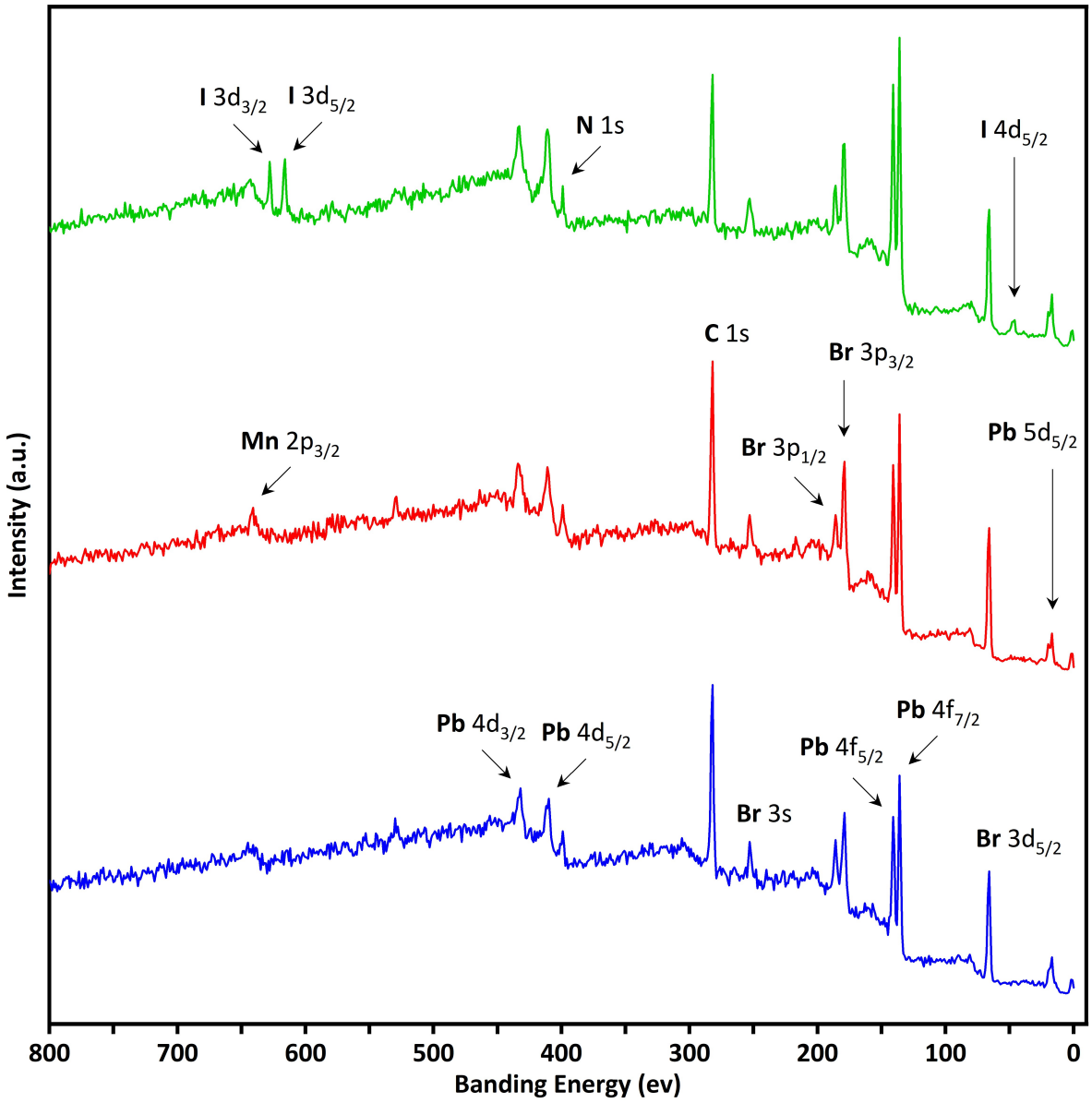

Figure S4. X-ray photoelectron spectroscopy signals of colloidal aerogels of $(C_6H_5\text{-}CH_2\text{-}CH_2\text{-}NH_3)_2PbBr_3I_1$ (upper curve, depicted in green), $(C_6H_5\text{-}CH_2\text{-}CH_2\text{-}NH_3)_2Pb_{0.977}Mn_{0.023}Br_4$ (middle curve, depicted in red), and $(C_6H_5\text{-}CH_2\text{-}CH_2\text{-}NH_3)_2PbBr_4$ (lower curve, blue-colored) perovskite nanoplatelets.

$(C_6H_5\text{-}CH_2\text{-}CH_2\text{-}NH_3)_2Pb_{0.977}Mn_{0.023}Br_4$

BET specific surface area: 4.46 m^2/g

BJH adsorption average pore width: 18.5 nm

$(C_6H_5\text{-}CH_2\text{-}CH_2\text{-}NH_3)_2PbBr_3I_1$

BET specific surface area: 1.87 m^2/g

BJH adsorption average pore width: 9.0 nm

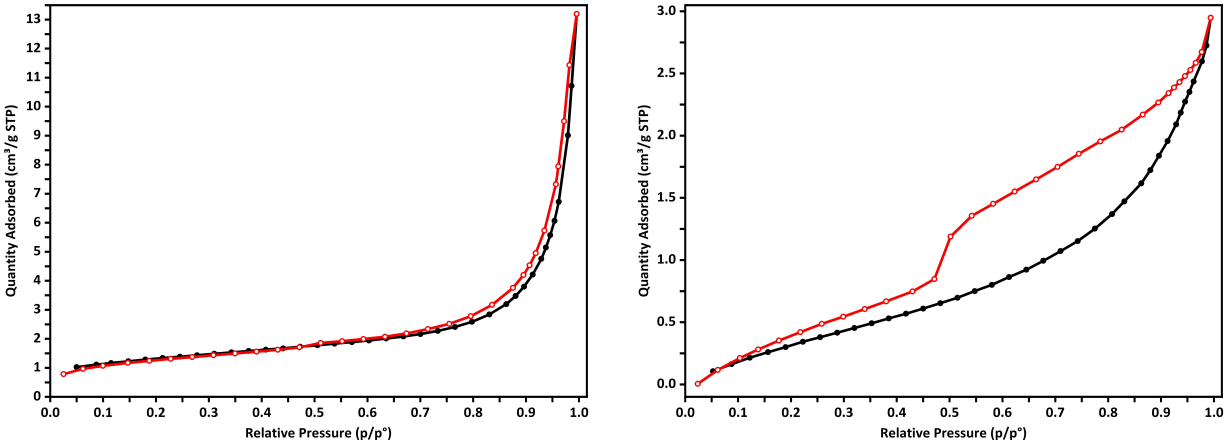

Figure S5. Nitrogen adsorption-desorption isotherms of colloidal aerogels of $(C_6H_5\text{-}CH_2\text{-}CH_2\text{-}NH_3)_2Pb_{0.977}Mn_{0.023}Br_4$ and $(C_6H_5\text{-}CH_2\text{-}CH_2\text{-}NH_3)_2PbBr_3I_1$ perovskite nanoplatelets.

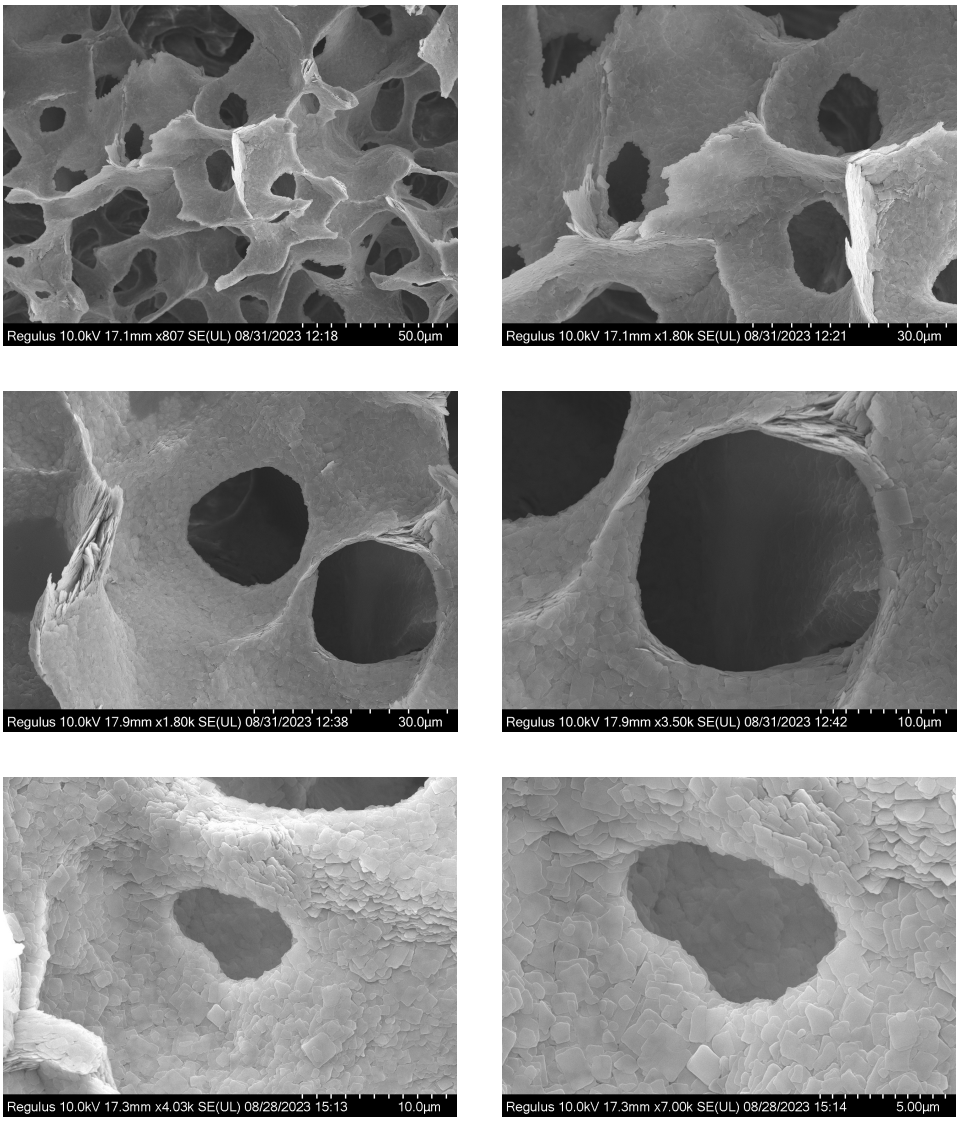

Figure S6. Cross-sectional scanning electron microscopy images of $(C_6H_5\text{-}CH_2\text{-}CH_2\text{-}NH_3)_2PbBr_4$ aerogels.

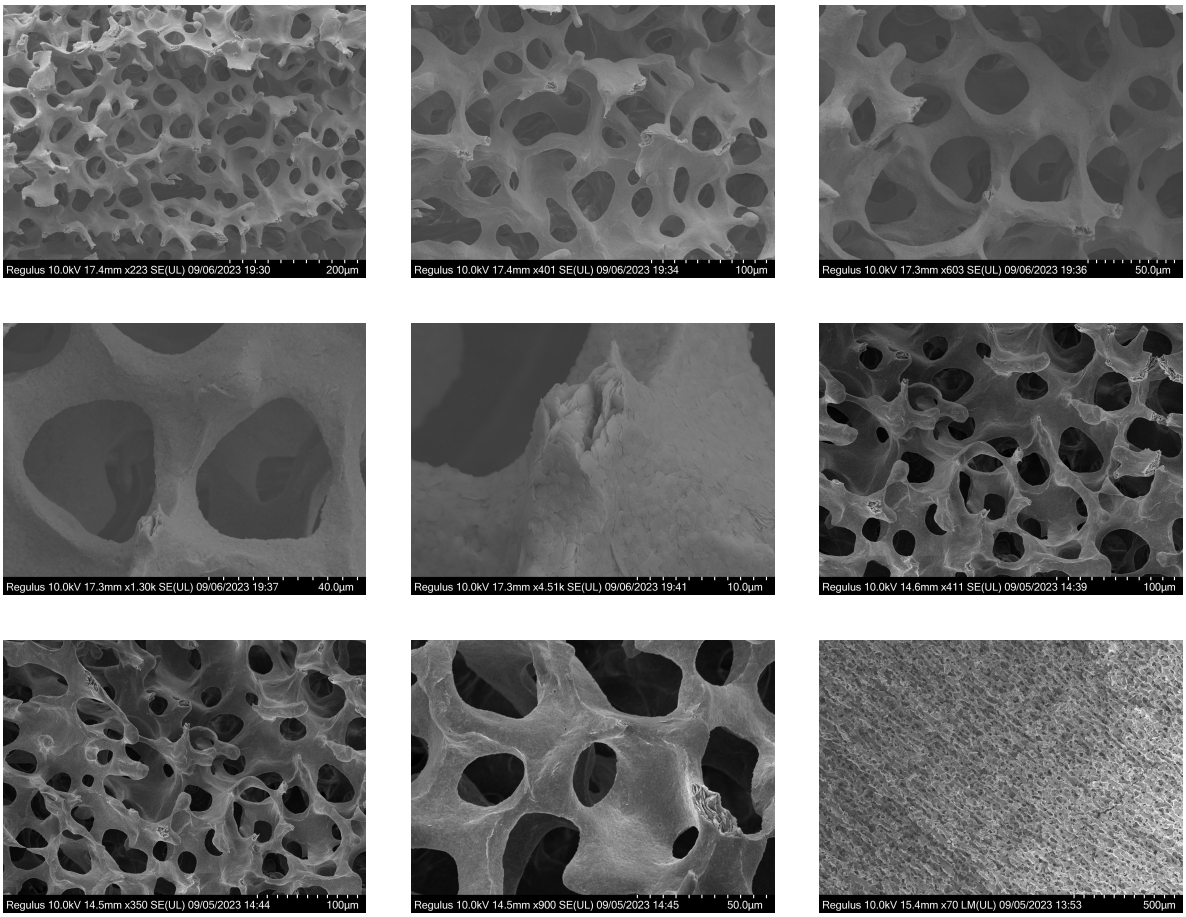

Figure S7. Cross-sectional scanning electron microscopy images of $(C_6H_5\text{-}CH_2\text{-}CH_2\text{-}NH_3)_2Pb_{0.977}Mn_{0.023}Br_4$ aerogels.

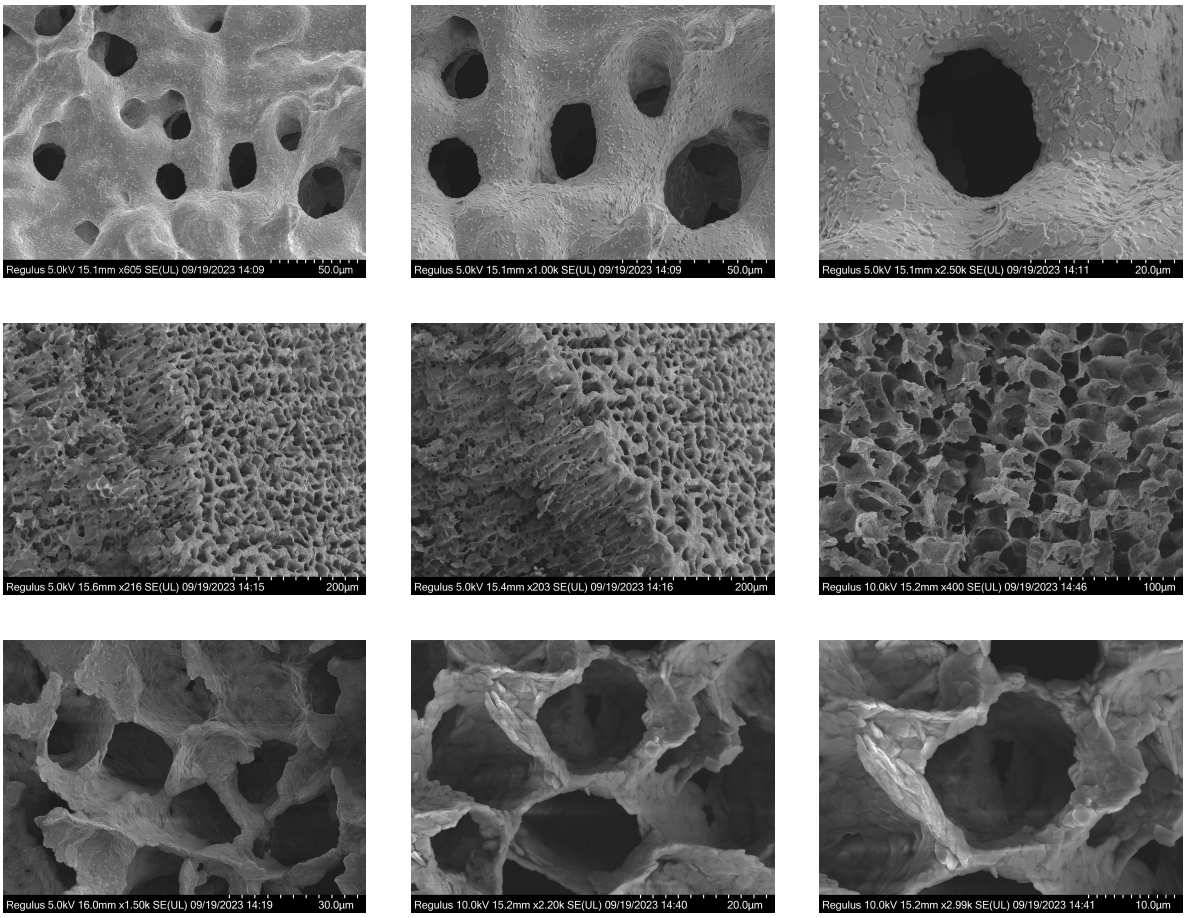

Figure S8. Cross-sectional scanning electron microscopy images of $(C_6H_5\text{-}CH_2\text{-}CH_2\text{-}NH_3)_2PbBr_3I_1$ aerogels.

$(C_6H_5\text{-}CH_2\text{-}CH_2\text{-}NH_3)_2Pb_{0.977}Mn_{0.023}Br_4$

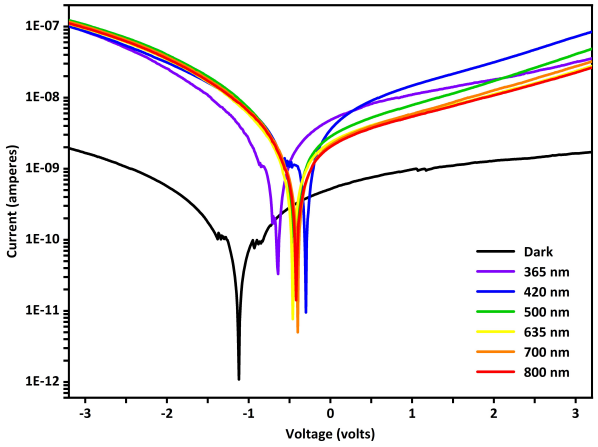

$(C_6H_5\text{-}CH_2\text{-}CH_2\text{-}NH_3)_2PbBr_3I_1$

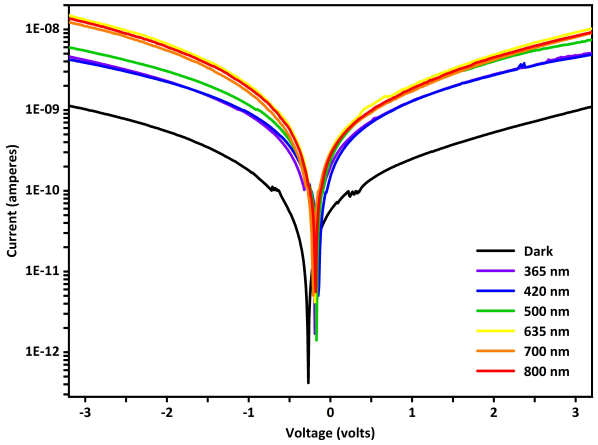

Figure S9. Current-voltage characteristics of $(C_6H_5\text{-}CH_2\text{-}CH_2\text{-}NH_3)_2Pb_{0.977}Mn_{0.023}Br_4$ and $(C_6H_5\text{-}CH_2\text{-}CH_2\text{-}NH_3)_2PbBr_3I_1$ perovskite aerogels under 0.18 mW/mm^2 illumination.